Journal of Cerebral Blood Flow & Metabolism (2012) 32, 1737–1746

www.jcbfm.com

Increase of 20-HETE synthase after brain ischemia in rats revealed by PET study with ^{11}C-labeled 20-HETE synthase-specific inhibitor

Toshiyuki Kawasaki[1,2], Toshiyuki Marumo[3], Keiko Shirakami[1], Tomoko Mori[1], Hisashi Doi[1], Masaaki Suzuki[1], Yasuyoshi Watanabe[1], Shigeyuki Chaki[3], Atsuro Nakazato[4], Yukio Ago[2], Hitoshi Hashimoto[5,6,7], Toshio Matsuda[2,6], Akemichi Baba[5] and Hirotaka Onoe[1]

[1]*RIKEN, Center for Molecular Imaging Science, Kobe, Japan;* [2]*Laboratory of Medicinal Pharmacology, Graduate School of Pharmaceutical Sciences, Osaka University, Suita, Japan;* [3]*Molecular Function and Pharmacology Laboratories, Taisho Pharmaceutical Co., Ltd., Saitama, Japan;* [4]*Strategic Planning of Drug Discovery, R&D Headquarters of Pharmaceutical Operation, Taisho Pharmaceutical Co., Ltd., Saitama, Japan;* [5]*Laboratory of Molecular Neuropharmacology, Graduate School of Pharmaceutical Sciences, Osaka University, Suita, Japan;* [6]*United Graduate School of Child Development, Osaka University, Kanazawa University and Hamamatsu University School of Medicine, Osaka University, Suita, Japan;* [7]*Department of Molecular Pharmaceutical Science, Graduate School of Medicine, Osaka University, Suita, Japan*

20-Hydroxyeicosatetraenoic acid (20-HETE), an arachidonic acid metabolite known to be produced after cerebral ischemia, has been implicated in ischemic and reperfusion injury by mediating vasoconstriction. To develop a positron emission tomography (PET) probe for 20-HETE synthase imaging, which might be useful for monitoring vasoconstrictive processes in patients with brain ischemia, we synthesized a ^{11}C-labeled specific 20-HETE synthase inhibitor, *N*′(4-dimethylamino-hexyloxy)phenyl imidazole ([^{11}C]TROA). Autoradiographic study showed that [^{11}C]TROA has high-specific binding in the kidney and liver consistent with the previously reported distribution of 20-HETE synthase. Using transient middle cerebral artery occlusion in rats, PET study showed significant increases in the binding of [^{11}C]TROA in the ipsilateral hemisphere of rat brains after 7 and 10 days, which was blocked by co-injection of excess amounts of TROA (10 mg/kg). The increased [^{11}C]TROA binding on the ipsilateral side returned to basal levels within 14 days. In addition, quantitative real-time PCR revealed that increased expression of 20-HETE synthase was only shown on the ipsilateral side on day 7. These results indicate that [^{11}C]TROA might be a useful PET probe for imaging of 20-HETE synthase in patients with cerebral ischemia.
Journal of Cerebral Blood Flow & Metabolism (2012) **32,** 1737–1746; doi:10.1038/jcbfm.2012.68; published online 6 June 2012

Keywords: 20-HETE; 20-HETE synthase; ischemia; microglia; PK11195; transient middle cerebral artery occlusion

Introduction

Arachidonic acid (AA) is one of the most abundant fatty acids in the brain. On physiologic and pathologic stimulation, AA-selective lipases release the fatty acid from membrane phospholipid pools and make it available for its oxidation by the enzymes of the AA cascade (Abe *et al*, 1987; Pilitsis *et al*, 2003). The AA cascade mainly consists of cyclooxygenases and lipoxygenases (Capdevila *et al*, 1992), the metabolites of which are known to have abundant biologic functions in signal transduction and cell–cell interactions. Recently, in addition to these enzymes, monooxygenases belonging to the cytochrome P450 (CYP) family also metabolize AA, although the biologic function of its metabolites remains unknown.

Correspondence: Hirotaka Onoe, Functional Probe Research Laboratory, RIKEN, Center for Molecular Imaging Science, 6-7-3 Minatojima-Minamimachi, Chuo-ku, Kobe, Hyogo 650-0047, Japan.
E-mail: hiro.onoe@riken.jp
This study was supported in part by the 'Molecular Imaging Research Program' of the Ministry of Education, Culture, Sports, Science, and Technology of Japan.
Received 27 January 2012; revised 1 May 2012; accepted 2 May 2012; published online 6 June 2012

20-Hydroxyeicosatetraenoic acid (20-HETE) is one of the AA metabolites produced by some CYP isozymes, which we termed 20-HETE synthase, mainly by CYP4A and 4F (Laethem *et al*, 1992; Roman, 2002). It has been reported that 20-HETE acts as a potent vasoconstrictor of cerebral microvessels (Harder *et al*, 1994), and has an important role in the autoregulation of cerebral blood flow (Gebremedhin *et al*, 2000). 20-Hydroxyeicosatetraenoic acid has also been reported to induce the formation of oxygen radicals by interacting with nicotinamide adenine dinucleotide phosphate-oxidase and nitric oxide synthase (Wang *et al*, 2006; Cheng *et al*, 2008; Medhora *et al*, 2008). Previously, we reported that brain and plasma 20-HETE levels were significantly increased in the rat transient middle cerebral artery occlusion (tMCAO) model (Tanaka *et al*, 2007), and inhibition of 20-HETE synthesis by *N*-(3-chloro-4-morpholin-4-yl)phenyl-*N*′-hydroxyimido formamide (TS-011), a selective inhibitor of CYP4s, improved the autoregulatory dysfunction in the peri-infarct microcirculation and the neurologic outcomes in rat and monkey stroke models by reducing the infarct volume of the brain after ischemia (Miyata *et al*, 2005; Omura *et al*, 2006; Tanaka *et al*, 2007; Marumo *et al*, 2010). However, 20-HETE is also known to be involved in the angiogenesis induced by vascular endothelial growth factor, which is known to be upregulated in the ischemic brain after stroke for a repair process (Kovács *et al*, 1996; Plate *et al*, 1999; Zhang *et al*, 2002). 20-Hydroxyeicosatetraenoic acid synthase may exert a double-edged role in the ischemic brain by exacerbating neuronal injury at early phase, whereas the angiogenic effect is achieved at recovery phase. Thus, 20-HETE might be involved in both pathologic and repair processes in the brain after stroke. Therefore, monitoring of 20-HETE synthase after ischemic stroke may shed light on the time course and progress of brain injury and help physicians to decide on the best strategy for medical treatment after ischemic stroke.

Molecular imaging by positron emission tomography (PET) with radiopharmaceuticals enables noninvasive quantitative evaluation of physiologic biomarkers, such as receptors and enzymes, with super high sensitivity. PET, with specific and selective probes, allows three-dimensional visualization of the molecular changes relating to the physiologic and pathologic functions *in vivo*. To investigate the precise pathophysiologic role of 20-HETE synthase and the therapeutic effects of 20-HETE synthase inhibitors on ischemic stroke, we have synthesized a ^{11}C-labeled specific 20-HETE synthase inhibitor, *N*′(4-dimethylaminohexyloxy)-phenyl imidazole ([^{11}C]TROA) as a PET probe for visualizing 20-HETE synthase function in the living brain. In addition, with [^{11}C]TROA we performed longitudinal PET imaging using a rat model of tMCAO, and revealed the upregulation of 20-HETE synthase after ischemia.

Materials and methods

Animals

This study was performed in accordance with the international standards for animal welfare and institutional guidelines and approved by the Animal Care and Use Committee of RIKEN Kobe Institute (MAH21-21). Adult male C57/BL6 mice (7–8 weeks old) and Wistar rats (7–8 weeks old) were purchased from Japan SLC (Shizuoka, Japan). The mice and rats were housed three or four to a cage, under a 12-hour light–dark cycle (lights off at 2000 hours) at $23 \pm 1\,^{\circ}$C and $60 \pm 5\%$ humidity, and were allowed access to food and water *ad libitum*. We used 16 mice and 33 rats in total (in mice, *in vitro* binding experiments: $n = 4$ and *in vivo* biodistribution: $n = 12$; and in rats, PET studies: $n = 7$, *in vivo* biodistribution: $n = 12$, immunohistochemistry: $n = 4$, RT-PCR: $n = 5$ and enzyme-linked immunosorbent assay (ELISA): $n = 5$). In the PET studies, we used same three rats for [^{11}C]TROA and [^{11}C]PK11195 PET studies, in which PET study of rats are conducted twice a day at all time points.

Characterization of the Effects of TROA

The binding and enzyme assays were performed as a contract study by CEREP (Celle l'Evescault, France). A list of the assays used is provided in Supplementary Table 1. All experiments were performed at least in duplicate.

Chemicals

The [^{11}C]TROA (Supplementary Figure 1) was prepared using the reaction of a TROA precursor (*N*′(4-methylaminohexyloxy)phenyl imidazole; 0.5 mg) in DMF (250 μl) with [^{11}C]CH_3I produced by a cyclotron (HM12; Sumitomo Heavy Industry, Tokyo, Japan). The precursor and standard TROA were synthesized according to the procedures described by Nakamura *et al* (2004). Radiochemical purities were $>95\%$, and specific activities were 55.7 ± 41.4 GBq/μmol (mean ± standard deviation) at the time of injection. The ^{11}C-labeled PK11195 was prepared according to the procedures described by Cui *et al* (2009).

In Vitro Autoradiography

Kidney, liver, and brain tissues obtained from individual mice were rapidly frozen in powdered dry ice, and were mounted on cryostat chucks. Coronal sections (20 μm) were cut and thaw-mounted onto gelatin-coated slides. Sections were stored at $-20\,^{\circ}$C before the experiment. Tissue sections were pre-incubated in assay buffer (50 mmol/L Tris-HCl/0.9% saline (NaCl), buffered at pH 7.6) for 30 min, and then rapidly dried under a stream of cool air. The sections were incubated for 30 min in assay buffer with either 1–2 nmol/L [^{11}C]TROA alone or in combination with unlabeled 20-HETE synthase inhibitors (10 μmol/L). Following incubation, the sections were rinsed by immersing in an assay buffer for 30 seconds, followed by another 30 seconds rinse in fresh buffer and a final 30 seconds rinse

in ice-cold purified water, then quickly dried under a stream of warm air. Tissue sections were juxtaposed to an imaging plate (BAS MS2040, Fuji Photo Film, Tokyo, Japan) for 40 min. Quantitative autoradiogram analysis was performed using densitometry and a Bio-Image Analyzer FLA7000 (Fuji Photo Film). The radioactivity concentrations of each region were quantified and expressed as photo-stimulated luminescence/area (mm^2).

Autoradiography

After a bolus injection of [^{11}C]TROA (20 ± 3 MBq per animal) into the tail vein, the mice were killed 30 minutes later by rapid decapitation. For the blocking study, mice were injected with unlabeled 20-HETE synthase inhibitors (10 mg/kg) via the tail vein 5 minutes before [^{11}C]TROA injection. Autoradiograms were prepared by exposing the brain and kidney slices (1 mm) to BAS-SR phosphor-imaging plates (Fuji Photo Film) for 40 minutes. Cassettes were then opened under subdued light and the plates were measured with a FLA-7000 IP reader (Fuji Photo Film). The tissue radioactivity was measured using a 1470 WIZARD Automatic Gamma Counter (PerkinElmer, Waltham, MA, USA) and expressed as percent injected dose (ID) per gram of tissue and normalized for injected radioactivity.

In Vivo Biodistribution

Adult male Wistar rats were anesthetized with 1.5% isoflurane and [^{11}C]TROA (approximately 60 ± 3 MBq/animal) was injected via intravenous tail vein. Displacement study was performed by injecting an excess (10 mg/kg) of unlabeled TROA 20 minutes after the tracer injection. Rats were killed at 10 and 60 minute after injection, $n = 4$ rats for each time point. Samples of blood, brain, lung, kidney, and liver were collected and all samples were counted in a 1470 WIZARD Automatic Gamma Counter. Tissues were weighed and the percentage of the ID per gram of tissue (%ID/g) was calculated.

Middle Cerebral Artery Occlusion Model in Rats

Transient occlusion of the middle cerebral artery (MCA) was induced by the intraluminal filament method as previously described (Nagasawa and Kogure, 1989). An 18-mm long piece of 4–0 nylon suture coated with silicon was introduced into the right internal carotid artery to occlude the origin of the right MCA. Anesthesia was withdrawn and successful occlusion judged by the appearance of hemiparesis. One hour after occlusion of the MCA, the rats were reanesthetized and the suture withdrawn to allow reperfusion.

PET Studies

Rats were anesthetized with a mixture of 1.5% isoflurane and nitrous oxide/oxygen (7:3) and then placed on the PET scanner gantry (microPET Focus 220, Siemens, Knoxville, TN, USA). The PET scanner has a spatial resolution of 1.4 mm in full-width at half-maximum at the center of the field of view of 220 mm in diameter and an axial extent of 78 mm in length. After intravenous bolus injection of [^{11}C]TROA or [^{11}C]PK11195 (ca 60 MBq per animal) by means of a venous catheter inserted into the tail vein, a 90-minutes emission scan was performed. In the blocking experiment, we performed two PET scans of each animal. Seven and eight days after MCAO, rats were injected with vehicle and unlabeled compound (10 mg/kg) 5 minutes before [^{11}C]TROA injection, respectively. Emission data were acquired in list mode, and the data were reconstructed with standard two-dimensional filtered back projection (Ramp filter, cutoff frequency at 0.5 cycles per pixel). For the PET study with MCAO in the rat brain, regions of interest were placed on the ipsilateral and contralateral hemispheres and the cerebellum by using image-processing software (Pmod ver. 3.0, PMOD Technologies, Zurich, Switzerland) with reference to the rat magnetic resonance image. Regional uptake of radioactivity in the brain was decay-corrected to the injection time and expressed as the standardized uptake value (SUV).

PET Analysis

Reconstructed images were processed with Pmod software. Standardized uptake value summation images 30–90 minutes after injection of [^{11}C]PK11195 and [^{11}C]TROA were obtained by normalizing tissue radioactivity concentration by ID and body weight. To elucidate the quantitative [^{11}C]TROA binding to 20-HETE synthase in the brain, we calculated binding potentials (BPs) using the multilinear reference-tissue model 2 in which the cerebellum was used as the reference region (Ichise *et al*, 2003).

Immunohistochemistry

The animals were perfused through the aorta with 150 mL of 10 mmol/L PBS, followed by 300 mL of a cold fixative consisting of 4% paraformaldehyde in 100 mmol/L phosphate buffer under deep anesthesia with sodium pentobarbital (50 mg/kg, intraperitoneally). After perfusion, the brains were quickly removed and post-fixed for 2 days in 4% paraformaldehyde in 100 mmol/L phosphate buffer and then transferred to a 20% sucrose solution in 100 mmol/L phosphate buffer for 3 days at 4 °C. The brain pieces were cut into 20-μm-thick sections using a cryostat and sections were thaw-mounted onto gelatin-coated slides. After several washes, the sections were incubated for 1 day at room temperature with rabbit polyclonal primary antibodies against glial fibrillary acidic protein (GFAP; 1:1,000; Santa Cruz Biotechnology, Santa Cruz, CA, USA) and CYP 4A (1:100; Thermo scientific, Waltham, MA, USA), and mouse monoclonal primary antibodies against CD11b (1:100; AbDSerotec, Oxford, UK), GFAP (1:1,000; Chemicon International, Temecula, CA, USA), and neuron-specific nuclear protein (NeuN; 1:500; Chemicon International). The primary antibodies were detected with an anti-mouse IgG antibody conjugated with Cy-3 and an anti-rabbit IgG antibody conjugated with Cy-2 (1:500; Jackson ImmunoResearch Laboratories, PA, USA) for 2 hour at

room temperature. Fluorescence was then detected using a Digital Eclipse C1 system equipped with a TE2000-E microscope (Nikon, Tokyo, Japan).

Quantitative Reverse Transcriptase-PCR

The changes in the expression of some of the most important 20-HETE synthases were confirmed by quantitative real-time reverse transcriptase-PCR (qPCR). Seven days after tMCAO, the animals were perfused through the aorta with 150 mL of 10 mmol/L PBS. Tissue samples of the ipsilateral infracted brain region including cortex and striatum, and corresponding contralateral region were collected and were immediately frozen in liquid nitrogen and stored at −80 °C until RNA extraction. Total RNA was extracted from brain tissue using SV Total RNA Isolation System (Promega Corporation, Madison, WI, USA). The complementary DNA was synthesized from 1 μg of total RNA using reverse transcriptase and a Superscript III kit (Invitrogen, Gaithersburg, MD, USA). The qPCR for total complementary DNA was performed in the ABI Prism 7,000 sequence detection system, using the standard protocols with the GoTaq qPCR Master Mix (Promega). The qPCR assays were performed in duplicate. The relative expression of Cyp4a1, 4a8, 4f1, 4f4, 4f5, and 4f6 mRNA was calculated after normalization to glyceraldehyde-3-phosphate dehydrogenase mRNA. Sequences of the forward (F) and reverse (R) primers used for the real-time PCRs are as follows: rat Cyp4a1: F: 5′-GTTCTACCTGCAAAGGCAA TGG-3′, R: 5′-TGCCCAAAGAACCAGTGGAA-3′; rat Cyp4a2: F: 5′-GTGGAATCTCCTGGGTTTTCTATG-3′, R: 5′-TGGTG GTGTAAGGCATCTGG-3′; rat Cyp4a3: F: TCTCAGGGAG CAAAACACGA-3′, R: 5′-CAACAGGAGCAAACCATAAC CA-3′; rat Cyp4a8: F: 5′-GACAGCACAAGACAGCTCCA-3′, R: 5′-AGGTGAACAAGGTGAGAAGAAAGAA-3′; rat Cyp4f1: F: 5′-CCCCCAAGGCTTTTTGATG-3′, R: 5′-GAGCGCAACGG CAGCT-3′; rat Cyp4f4: F: 5′-CAGGTCTGAAGCAGGTAACT AAGC-3′, R: 5′-CCGTCAGGGTGGCACAGAGT-3′; rat Cyp4f5: F: 5′-AGGATGCCGTGGCTAACTG-3′, R: 5′-GGCTCCAAG CAGCAGAAGA-3′; rat Cyp4f6: F: 5′-TGATGAAGAACAAC-GAGGAAGG-3′, R: 5′-TTGGAGCAGGGGAGCAA-3′; and rat glyceraldehyde 3-phosphate dehydrogenase: F: 5′-GAACATC ATCCCTGCATCCA-3′, R: 5′-CCAGTGAGCTTCCCGTTCA-3′.

Enzyme-Linked Immunosorbent Assay

Seven days after tMCAO, the animals were perfused through the aorta with 150 mL of 10 mmol/L PBS. The ipsilateral infracted brain region including cortex and striatum, and corresponding contralateral region were collected and were immediately frozen in liquid nitrogen and stored at −80 °C. The brains were homogenized in 2 mL of H_2O containing 5 μg triphenylphosphine and added 4 μL acetic acid to acidify the homogenate. The homogenate was then extracted twice with 2 mL of ethyl acetate. After drying the organic phase with nitrogen gas, the dried residue were dissolved in 10 μL ethanol. The amount of 20-HETE in the brain was then determined using an ELISA kit for 20-HETE according to the manufacturer's instructions (Detroit R&D, Detroit, MI, USA).

Statistical Analysis

All data were expressed as mean ± standard deviation (s.d.). For PET studies, the statistical differences were analyzed using two-way analysis of variance (ANOVA) followed by the Tukey–Kramer test. For qPCR studies, the results were shown as fold change versus the contralateral side, and the data were evaluated using one-sample *t*-test. Statistical analyses were performed using a software package Statview 5.0J for Apple Macintosh computer (SAS Institute, Cary, NC, USA). A value of $P<0.05$ was considered statistically significant.

Results

Characterization of the Effects of TROA on Receptors and Enzymes

Binding and inhibitory activities of TROA to several kinds of neuroreceptors and enzymes were investigated. The effects of TROA on receptors and enzymes are summarized in Supplementary Table 1. In a previous paper, Nakamura *et al* (2004) reported that an imidazole derivative TROA exhibited a potent and selective inhibition to 20-HETE synthase. TROA strongly inhibits 20-HETE synthase with an IC_{50} value of 2.2 nmol/L, which is 180-fold to 15,000-fold over that of CYP1A2, 2C9, 2C19, 2D6, and 3A4, and has no significant effect on the activity of any of other kinds of enzymes tested. In addition, TROA at a concentration of 1 μmol/L exhibited little or no affinity for any of the receptors tested. Therefore, TROA has highly selective inhibitory effects on 20-HETE synthase but shows a broad range of low binding activity to receptors.

Autoradiography and Biodistribution

Figure 1 shows the results of quantitative autoradiographic studies on [^{11}C]TROA binding in the mouse liver, kidney, and brain sections. Binding of [^{11}C]TROA was high in the liver and kidney (Figures 1A and 1C), but low in the brain (Figure 1E). Co-incubation with unlabeled TROA at 10 μmol/L completely eliminated the radioactivity binding to the liver, kidney, and also brain sections (Figures 1B, 1D and 1F). Quantitative data show a dose-dependent blocking effect of unlabeled TROA (Figures 1G–I). *Ex vivo* autoradiographic studies in mice also showed high accumulation of radioactive compound in the kidney (Figure 2A) and low in the brain (Figure 2D). Preinjection of unlabeled TROA at a dosage of 10 mg/kg (Figures 2B, E) or another 20-HETE synthase-selective inhibitor TS-011 at a dose of 10 mg/kg (Figures 2C, F), resulted in a strong and significant blocking in the kidney, but had little effect on [^{11}C]TROA accumulation in the brain (Figure 2G). Biodistribution data, acquired 10 and 60 minutes after injection of [^{11}C]TROA, are presented in Supplementary Table 2. The highest uptake of [^{11}C]TROA radioactivity was found in the kidney. In addition, the liver exhibited high uptake of radioactivity. Displacement studies were performed by injecting excess amounts of unlabeled TROA (10 mg/kg) 20 minutes after [^{11}C]TROA injection. Significant reduc-

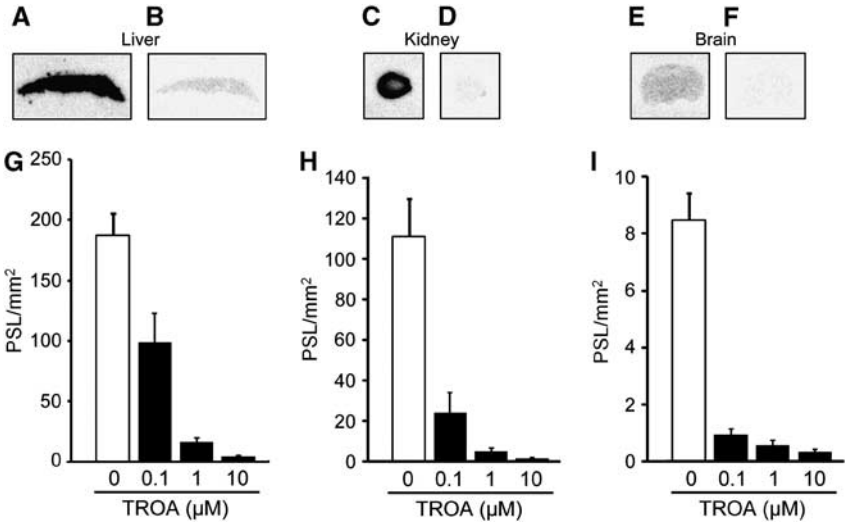

Figure 1 ^{11}C-labeled *N*′(4-dimethylaminohexyloxy)phenyl imidazole ([^{11}C]TROA) binding using autoradiography. (**A**, **C**, **E**) Liver, kidney, and brain sections from naive mice were incubated with 1–2 nmol/L [^{11}C]TROA for 30 min. (**B**, **D**, **F**) Nonspecific binding was determined by incubation with 10 μmol/L unlabeled TROA. (**G-I**) Quantitative data showed [^{11}C]TROA binding measured using densitometry of autoradiography images. Specific binding was determined by incubation with 0.1–10 μmol/L unlabeled TROA. Data are expressed as the mean ± s.d. from four mice. PSL, photo-stimulated luminescence.

tions of radioactivity concentration were observed for the 20-HETE synthase-rich organs (kidney, liver, and lung).

PET Study

Figure 3 shows representative PET images and time-activity curves of [^{11}C]TROA in a naive brain and in a rat brain 7 days after tMCAO. In the naive rat brain, the peak [^{11}C]TROA radioactivity was high in the forebrain (1.93 SUV; right and left hemisphere regions of interests), compared with the cerebellum (1.66 SUV). The peak [^{11}C]TROA radioactivity markedly increased on the ipsilateral side (2.46 SUV) 7 days after tMCAO. Figure 4 shows representative BP images of [^{11}C]TROA in the tMCAO rat brain, which were analyzed using the multilinear reference-tissue model 2 using the time-activity curve from the cerebellum as a reference. The BP values in the ipsilateral and contralateral hemispheres were evaluated at 3, 7, 10, 14, and 28 days after tMCAO (Figure 4B). An increase in [^{11}C]TROA BP value in the ipsilateral hemisphere was detected at 3 days and peaked at 7 days after tMCAO. Repeated-measures two-way ANOVA revealed a significant main effect of tMCAO ($F_{(1,12)} = 122.522$, $P < 0.0001$) and time [$F_{(5,\ 12)} = 8.880$, $P = 0.0010$], and there was a significant interaction between the tMCAO and the time ($F_{(5,\ 12)} = 14.218$, $P = 0.0001$). We further examined the effect of co-injection of unlabeled TROA (10 mg/kg) with [^{11}C]TROA on the elevated BP value in the tMCAO rat brain (Figures 4C, D). Pretreatment of TROA significantly reduced the BP value on the ipsilateral but not on the contralateral side. Two-way ANOVA revealed a significant main effect of MCAO ($F_{(1,\ 8)} = 69.399$, $P < 0.0001$), and TROA treatment ($F_{(1,\ 8)} = 10.535$, $P = 0.0116$), and there was a significant interaction between tMCAO and TROA ($F_{(1,\ 8)} = 7.999$, $P = 0.0222$). Moreover, we compared the time course of activated microglia and astrocytes using [^{11}C]PK11195, a specific tracer for translocator protein, with that of [^{11}C]TROA accumulation. Figure 5 shows representative PET images of [^{11}C]PK11195 in the rat brain before and after the tMCAO. The accumulation pattern of [^{11}C]PK11195 in the ipsilateral side at 3 and 7 days after tMCAO was quite similar to that of [^{11}C]TROA. However, [^{11}C]PK11195 accumulated at significant levels even 1 month after tMCAO, during which [^{11}C]TROA accumulation returned almost to baseline levels. Repeated-measures two-way ANOVA revealed a significant main effect of tMCAO ($F_{(1,10)} = 316.554$, $P < 0.0001$) and time ($F_{(4,\ 10)} = 21.992$, $P < 0.0001$), and there was a significant interaction between tMCAO and time ($F_{(4,\ 10)} = 35.528$, $P < 0.0001$).

Immunohistochemistry

The activation of microglia and astrocytes in the ischemic brain tissue was confirmed by immunohistochemical studies. Figure 6 shows the time course of CD11b$^+$ microglia and GFAP$^+$ astrocytes at 1, 3, 7, and 14 days after tMCAO. Glial fibrillary acidic protein-immunoreactivity in the ischemic core decreased at 1, 3, and 7 days but increased at 14 days after tMCAO. In addition, CD11b$^+$ cells with an ameboid morphology in the ischemic region increased at 3 and 7 days and then decreased at 14 days at which time CD11b$^+$ cells with non-ameboid shape were detected, instead of the ameboid-shaped CD11b$^+$ cells (Figure 6D). To characterize CYP4A-expressing cell type at 7 days after tMCAO, we double stained the CYP4A-positive cells with CD11b, GFAP, or NeuN (Supplementary Figure 2). In the contralateral striatum, CYP4A-positive cells were mainly co-localized with NeuN-positive neuron

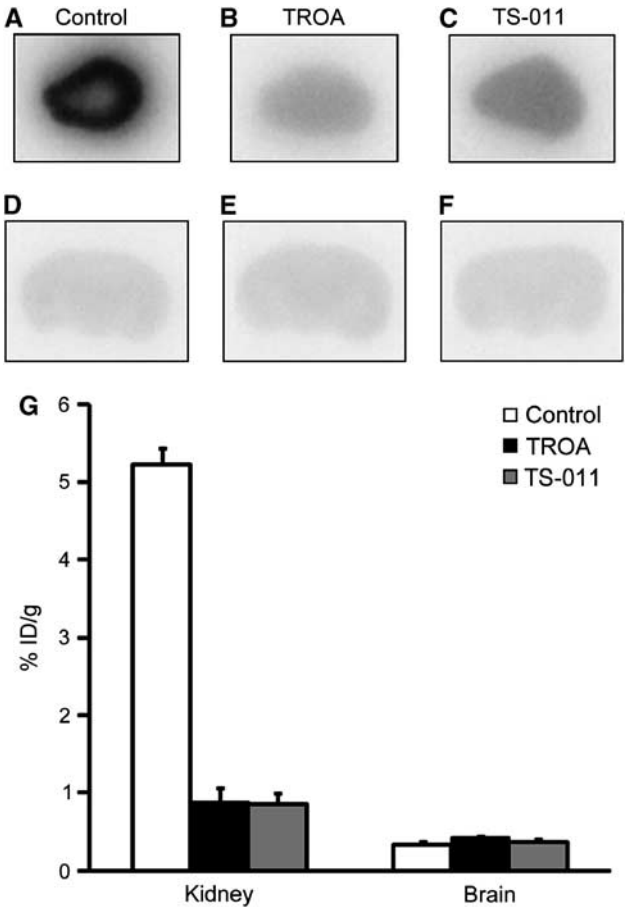

Figure 2 ^{11}C-labeled *N*′(4-dimethylaminohexyloxy)phenyl imidazole ([^{11}C]TROA) binding using autoradiography. Kidney and brain from control mice ($n = 4$) (**A**, **D**), unlabeled 10 mg/kg TROA pretreated mice ($n = 4$) (**B**, **E**), and unlabeled 10 mg/kg *N*-(3-chloro-4-morpholin-4-yl)phenyl-*N*′-hydroxyimido formamide (TS-011) pretreated mice ($n = 4$) (**C**, **F**). (**G**) Quantitative data showed [^{11}C]TROA binding measured using densitometry of autoradiography images. Each value is in percentage injected dose (ID) per gram tissue given as mean ± s.d.

but not with CD11b and GFAP. However, CYP4A immunoreactivity in the ipsilateral striatum was mainly observed in the activated microglia, whereas most of CYP4A-positive neurons were disappeared.

Quantitative Reverse Transcriptase-PCR and ELISA

A significant increase of [^{11}C]TROA binding was produced by tMCAO ipsilaterally, indicating the induction or activation of 20-HETE synthase in the region of the infarct that was observed 7 days after tMCAO. We therefore, examined the expression levels of Cyp4as and Cyp4fs mRNA 7 days after tMCAO. In the rat, four members of CYP4A subfamily, 4A1, 4A2, 4A3, and 4A8, and four members of CYP4F subfamily, 4F1, 4F4, 4F5, and 4F6, have been previously identified. After tMCAO, ipsilateral Cyp4a1, Cyp4f5, and Cyp4f6 mRNA expression increased significantly with no significant change in Cyp4a8, Cyp4f1, and Cyp4f4 (Figure 7A). In contrast, we could not detect the expression of Cyp4a2 and 4a3 mRNA in the brain of Wistar rats. To confirm increases in CYP4s activities relating to the level of Cyp4s mRNA, we measured 20-HETE contents in the brain after the tMCAO. The 20-HETE content in the ischemic hemisphere at 7 days after infarct was approximately three times higher than that in the contralateral hemisphere (14.4 ± 4.3 pg/g wet tissue versus 4.64 ± 0.63 pg/g wet tissue, $P < 0.01$; Figure 7B).

Discussion

This is the first paper demonstrating changes in 20-HETE synthase expression in a rat model of cerebral ischemia using [^{11}C]TROA that we synthesized as a specific PET tracer for 20-HETE synthase. First, we evaluated whether [^{11}C]TROA is a possible PET tracer for 20-HETE synthase. We found that specific binding of [^{11}C]TROA is high in the liver and kidney, but autoradiography revealed it is less specifically bound in the brain. This result is consistent with the

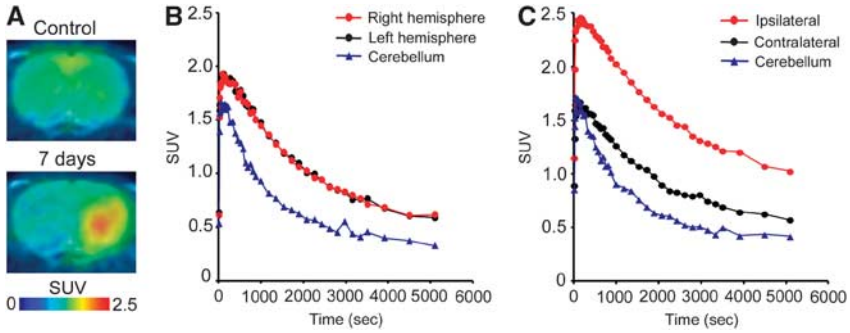

Figure 3 Representative positron emission tomography (PET) images and time-activity curves for ^{11}C-labeled *N*′(4-dimethylaminohexyloxy)phenyl imidazole of control and transient middle cerebral artery occlusion (tMCAO) rat brain. (**A**) PET images were co-registered with an magnetic resonance imaging (T1) rat template to anatomically localize the PET signal. (**B**, **C**) Standardized uptake value (SUV) was quantified in three region-of-interest areas defined in the right (ipsilateral) and left (contralateral) hemispheres and cerebellum of control and tMCAO rat brains.

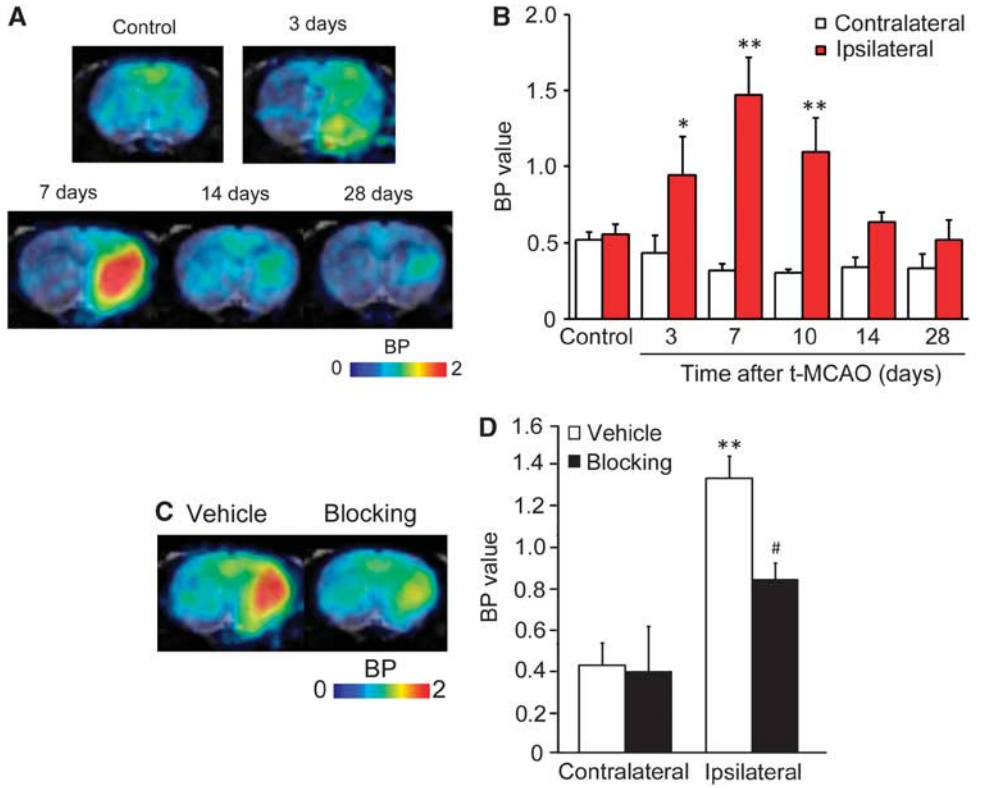

Figure 4 Binding potential (BP) images and BP values for ^{11}C-labeled *N*′(4-dimethylaminohexyloxy)phenyl imidazole ([^{11}C]TROA) of control and transient middle cerebral artery occlusion (tMCAO) rat brain. (**A**, **B**) The time course of the progression of the [^{11}C]TROA BP at 3 ($n = 3$), 7 ($n = 3$), 10 ($n = 3$) 14 ($n = 3$), and 28 ($n = 3$) days after tMCAO. Binding potential images and values were estimated using the multilinear reference-tissue model 2, in which the cerebellum was used as the reference region. The data represent the mean ± s.d. $^{*}P < 0.05$, $^{**}P < 0.01$ compared with the control group. (**C**, **D**) Blocking studies by injecting of vehicle ($n = 4$) at 7 days or 10 mg/kg TROA ($n = 4$) at 8 days. $^{**}P < 0.01$ compared with the vehicle-treated contralateral hemisphere, $^{\#}P < 0.05$ compared with vehicle-treated ipsilateral side.

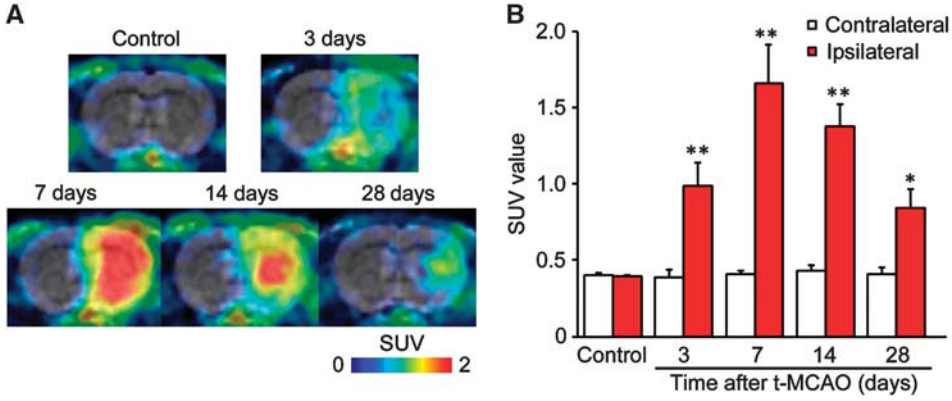

Figure 5 Representative positron emission tomography images and standardized uptake value (SUV) for [^{11}C]PK11195 of control and transient middle cerebral artery occlusion (tMCAO) rat brain. (**A**, **B**) The time course of the progression of the [^{11}C]PK11195 signal at 3 ($n = 3$), 7 ($n = 3$), 14 ($n = 3$), and 28 ($n = 3$) days after tMCAO. The data represent the mean ± s.d. $^{*}P < 0.05$, $^{**}P < 0.01$ compared with the control group.

expression levels of CYP4A and CYP4F isoforms in the individual tissue, which are known to produce 20-HETE as main metabolites of AA ω/(ω-1)-hydroxylases (Strömstedt *et al*, 1994; Kawashima and Strobel, 1995). Autoradiography also showed high-specific binding of [^{11}C]TROA in the kidney, but not in the brain suggesting a low expression level of 20-HETE synthase in brain parenchyma under

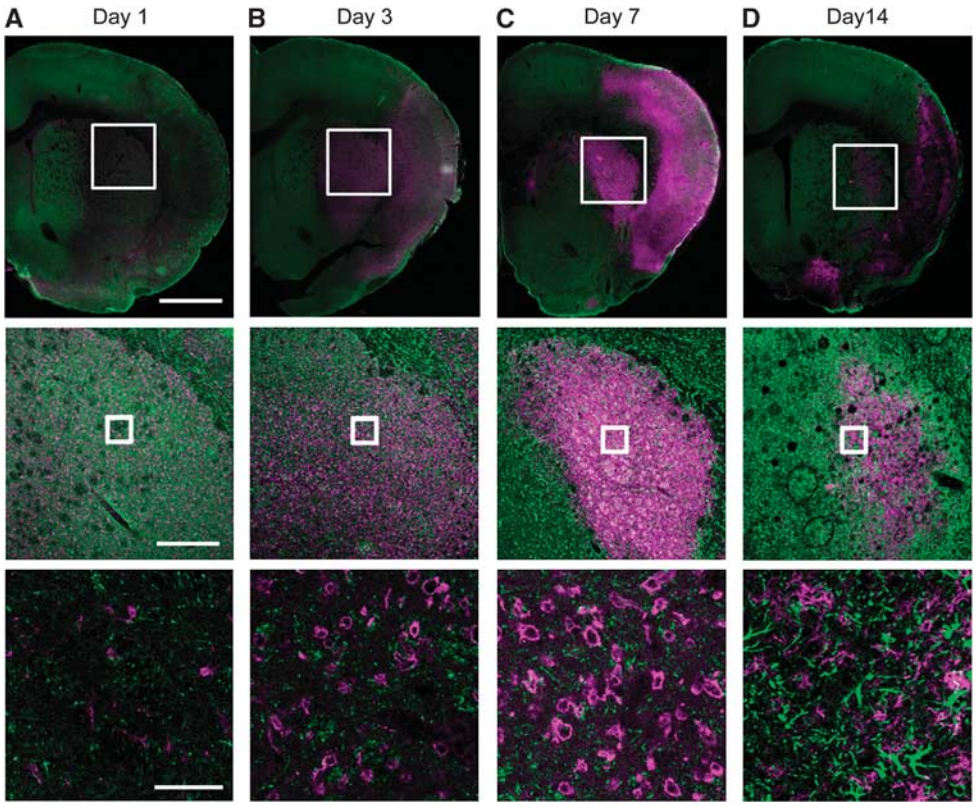

Figure 6 Double-immunofluorescence staining of CD11b (magenta) and glial fibrillary acidic protein (green) in the transient middle cerebral artery occlusion (tMCAO) rat brain. Representative photographs showing brain sections in the ischemic core region at 1, 3, 7, and 14 days after tMCAO (**A**–**D**). Scale bars in the top, middle, and bottom row are 1 mm, 300 μm, and 50 μm, respectively.

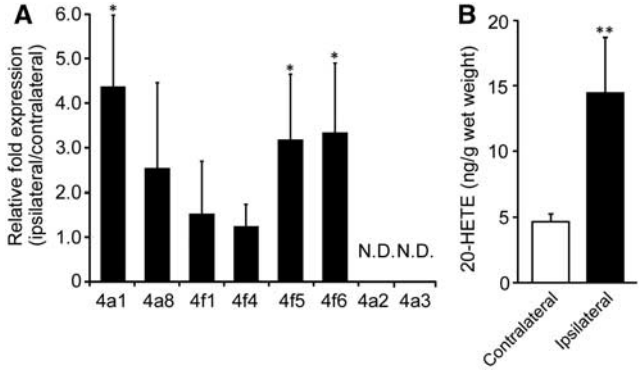

Figure 7 Cyp4a1, Cyp4a2, Cyp4a3, Cyp4a8, Cyp4f1, Cyp4f4, Cyp4f5, and Cyp4f6 mRNA levels were quantified by quantitative real-time reverse transcriptase-PCR (**A**). All data were normalized to the glyceraldehyde 3-phosphate dehydrogenase mRNA level and expressed as mRNA relative change, other than undetected Cyp4a2 and Cyp4a3. The values obtained from contralateral cortex were arbitrarily set to 1. Data are expressed as the mean ± s.d. from five rats. $*P < 0.05$. Amounts of 20-hydroxyeicosatetraenoic acid (20-HETE) in the ipsilateral or contralateral hemispheres at 7 day after transient middle cerebral artery occlusion were determined by enzyme-linked immunosorbent assay (**B**). Data are expressed as the mean ± s.d. from five rats. $**P < 0.01$ compared with the contralateral hemisphere. ND, not detected.

physiologic conditions. We also performed a [^{11}C]TROA PET study using a rat model of brain ischemia, and found elevation of specific binding in the tMCAO brain. In addition, we confirmed the upregulation of Cyp4a and Cyp4f expression and activity by using qPCR and ELISA. These findings indicate that [^{11}C]TROA PET is a potentially valuable tool for understanding changes in regional expression of 20-HETE synthase after cerebral ischemia.

To develop a PET probe for imaging of 20-HETE synthase, a potent and specific inhibitor for synthesis of 20-HETE is required. The IC_{50} value of TROA for the 20-HETE formation by human renal microsomes averaged 2.2 nmol/L, and this is comparable in magnitude to the reported IC_{50} for TS-011, which is known to be a potent inhibitor of 20-HETE formation and to reduce infarct size in the rat tMCAO model. In addition, TROA exhibited strong inhibitory activity against 20-HETE synthase more than 180-fold to over 15,000-fold selectivity compared with that toward other hepatic P450 enzymes. Therefore, [^{11}C]TROA is a promising compound that may help to evaluate the expression level of 20-HETE synthase *in vivo*.

In the present study, we also compared the time course of [^{11}C]TROA accumulation in the ischemic region to that of [^{11}C]PK11195 accumulation.

[^{11}C]PK11195 has been used as a radioligand for imaging of activated microglia and astrocytes in PET by binding to translocator protein that is expressed in these cells in the rat and human brains after cerebral ischemia. PET imaging showed increased [^{11}C]PK11195 binding at 3 and 28 days after cerebral ischemia and the accumulation pattern is similar to [^{11}C]TROA binding until day 7. Immunohistochemical studies show that the number of CD11b positive microglia in the ischemic core region increased progressively up to 7 days after tMCAO and decreased in the following weeks. In contrast, the upregulation of GFAP immunoreactivity was observed only in the penumbral region at 3 and 7 days after cerebral ischemia, but activated astrocytes started to increase in the ischemic core region at 14 days. The time course of [^{11}C]TROA accumulation is similar to that of microglial activation, suggesting that [^{11}C]TROA accumulation is mainly associated with the microglial activation in the early stages. Recent studies reported that CYP4A immunoreactivity was detected in neurons in hippocampus and putamen (Renic *et al*, 2012; Yang *et al*, 2012). In this study, CYP4A immunoreactivity was also detected in neurons in contralateral cortex and striatum. As there was an almost complete loss of NeuN-positive neurons in the infarcted core region at 7 days after tMCAO, CYP4A immunoreactivity was mostly observed in non-neuronal CNS cells including activated microglia. In addition, it is known that Cyp4fs were expressed in several cell types in the mouse brain, including neurons and microglia, and the expression level of Cyp4fs was increased only in the microglia after lipopolysaccharide and interferon-γ treatment (Snider *et al*, 2009; Sehgal *et al*, 2011). Therefore, it is also possible that ipsilateral Cyp4a and Cyp4f expression increased at 7 days after cerebral ischemia may be derived from the upregulation of this enzyme in activated microglia.

Recent studies have indicated that the levels of 20-HETE in the plasma and brain parenchyma of rats increased within 7.5 hours after tMCAO, and the inhibition of 20-HETE synthesis by TS-011 significantly reduced infarct volume in rats 24 hours after tMCAO. These results strongly suggest that transient 20-HETE elevation within hours after cerebral ischemia is involved in the development of brain infarction, and inhibition of 20-HETE elevation in the early stages is useful for the therapeutic treatment of ischemic stroke. In contrast, the present PET study with [^{11}C]TROA showed that a significant elevation of specific binding in the ipsilateral side was detected from 3 to 10 days, and peaked at 7 days after tMCAO. Vascular endothelial growth factor, which is known to induce angiogenesis, is upregulated ipsilateral to the tMCAO around the same day as the elevation of [^{11}C]TROA binding (Zhang *et al*, 2002). In fact, a marked increase in the levels of expression of some CYP4A and CYP4F isoforms was also observed on the ipsilateral side on the same day. Although the pathophysiologic role of CYP4A and CYP4F isoforms in the course of diseases remains to be determined, increases in 20-HETE synthesis mediated by these isoforms might be associated with the angiogenic response and neuroinflammation after stroke. CYP4As and CYP4Fs are known to inactivate proinflammatory leukotriene B4, which is one of the AA metabolites synthesized by 5-lipoxygenase and a principle mediator of the inflammatory response, initiating and amplifying the generation of cytokines and chemokines by metabolizing to 20-hydroxyl leukotriene B4 (Kalsotra and Strobel, 2006; Hsu *et al*, 2007; Crooks and Stockley, 1998). Sehgal *et al* (2011) reported that inhibition and induction of Cyp4Fs enhances and attenuates the inflammatory response triggered by lipopolysaccharide. Our data show that the reduction of microglial activation on the ipsilateral side was observed just after the peak time of [^{11}C]TROA binding. From this, it is possible to propose that CYP4As and CYP4Fs might be involved in modulating neuroinflammation through 20-HETE and/or 20-hydroxyl leukotriene B4 synthesis after cerebral ischemia. Further study is needed to address the detailed function of CYP4As and CYP4Fs on neurodegeneration, angiogenesis, and neuroinflammation after cerebral ischemia.

In summary, we have demonstrated that the expression of 20-HETE synthase is dynamically changed in the rat model of brain ischemia and [^{11}C]TROA provides quantitative information of 20-HETE synthase expression and distribution in the living brain. In addition, the time course of [^{11}C]TROA accumulation is coincident with microglial activation. As 20-HETE synthase is known to be expressed in microglia, and to modulate angiogenic and inflammatory responses, PET imaging of 20-HETE synthase is useful for monitoring disease progression, and inflammatory and repair processes after cerebral ischemia. Future studies of PET imaging with [^{11}C]TROA will provide quantitative information about the pathologic state of the brain during the course of the disease, which will prove useful for drug development targeting 20-HETE synthase.

Disclosure/conflict of interest

The authors declare no conflict of interest.

References

Abe K, Kogure K, Yamamoto H, Imazawa M, Miyamoto K (1987) Mechanism of arachidonic acid liberation during ischemia in gerbil cerebral cortex. *J Neurochem* 48: 503–9

Capdevila JH, Falck JR, Estabrook RW (1992) Cytochrome P450 and the arachidonate cascade. *FASEB J* 6:731–6

Cheng J, Ou JS, Singh H, Falck JR, Narsimhaswamy D, Pritchard KA, Jr, Schwartzman ML (2008) 20-Hydroxyeicosatetraenoic acid causes endothelial dysfunction

via eNOS uncoupling. *Am J Physiol Heart Circ Physiol* 294:1018–26

Crooks SW, Stockley RA (1998) Leukotriene B4. *Int J Biochem Cell Biol* 30:173–8

Cui Y, Takashima T, Takashima-Hirano M, Wada Y, Shukuri M, Tamura Y, Doi H, Onoe H, Kataoka Y, Watanabe Y (2009) ^{11}C-PK11195 PET for the *in vivo* evaluation of neuroinflammation in the rat brain after cortical spreading depression. *J Nucl Med* 50:1904–11

Gebremedhin D, Lange AR, Lowry TF, Taheri MR, Birks EK, Hudetz AG, Narayanan J, Falck JR, Okamoto H, Roman RJ, Nithipatikom K, Campbell WB, Harder DR (2000) Production of 20-HETE and its role in autoregulation of cerebral blood flow. *Circ Res* 87:60–5

Harder DR, Campbell WB, Roman RJ (1994) Role of cytochrome P-450 enzymes and metabolites of arachidonic acid in the control of vascular tone. *J Vasc Res* 32:79–92

Hsu MH, Savas U, Griffin KJ, Johnson EF (2007) Human cytochrome p450 family 4 enzymes: function, genetic variation and regulation. *Drug Metab Rev* 39:515–38

Ichise M, Liow JS, Lu JQ, Takano A, Model K, Toyama H, Suhara T, Suzuki K, Innis RB, Carson RE (2003) Linearized reference tissue parametric imaging methods: application to [^{11}C]DASB positron emission tomography studies of the serotonin transporter in human brain. *J Cereb Blood Flow Metab* 23:1096–112

Kalsotra A, Strobel HW (2006) Cytochrome P450 4F subfamily: at the crossroads of eicosanoid and drug metabolism. *Pharmacol Ther* 112:589–611

Kawashima H, Strobel HW (1995) cDNA cloning of three new forms of rat brain cytochrome P450 belonging to the CYP4F subfamily. *Biochem Biophys Res Commun* 217:1137–44

Kovács Z, Ikezaki K, Samoto K, Inamura T, Fukui M (1996) VEGF and flt. Expression time kinetics in rat brain infarct. *Stroke* 27:1865–72

Laethem RM, Laethem CL, Ding X, Koop DR (1992) P-450-dependent arachidonic acid metabolism in rabbit olfactory microsomes. *J Pharmacol Exp Ther* 262:433–8

Marumo T, Eto K, Wake H, Omura T, Nabekura J (2010) The inhibitor of 20-HETE synthesis, TS-011, improves cerebral microcirculatory autoregulation impaired by middle cerebral artery occlusion in mice. *Br J Pharmacol* 161:1391–402

Medhora M, Chen Y, Gruenloh S, Harland D, Bodiga S, Zielonka J, Gebremedhin D, Gao Y, Falck JR, Anjaiah S, Jacobs ER (2008) 20-HETE increases superoxide production and activates NAPDH oxidase in pulmonary artery endothelial cells. *Am J Physiol Lung Cell Mol Physiol* 294:902–11

Miyata N, Seki T, Tanaka Y, Omura T, Taniguchi K, Doi M, Bandou K, Kametani S, Sato M, Okuyama S, Cambj-Sapunar L, Harder DR, Roman RJ (2005) Beneficial effects of a new 20-hydroxyeicosatetraenoic acid synthesis inhibitor, TS-011 [N-(3-chloro-4-morpholin-4-yl) phenyl-N-hydroxyimido formamide], on hemorrhagic and ischemic stroke. *J Pharmacol Exp Ther* 314:77–85

Nagasawa H, Kogure K (1989) Correlation between cerebral blood flow and histologic changes in a new rat model of middle cerebral artery occlusion. *Stroke* 20:1037–43

Nakamura T, Kakinuma H, Umemiya H, Amada H, Miyata N, Taniguchi K, Bando K, Sato M (2004) Imidazole derivatives as new potent and selective 20-HETE synthase inhibitors. *Bioorg Med Chem Lett* 14:333–6

Omura T, Tanaka Y, Miyata N, Koizumi C, Sakurai T, Fukasawa M, Hachiuma K, Minagawa T, Susumu T, Yoshida S, Nakaike S, Okuyama S, Harder DR, Roman RJ (2006) Effect of a new inhibitor of the synthesis of 20-HETE on cerebral ischemia reperfusion injury. *Stroke* 37:1307–13

Pilitsis JG, Coplin WM, O'Regan MH, Wellwood JM, Diaz FG, Fairfax MR, Michael DB, Phillis JW (2003) Measurement of free fatty acids in cerebrospinal fluid from patients with hemorrhagic and ischemic stroke. *Brain Res* 985:198–201

Plate KH, Beck H, Danner S, Allegrini PR, Wiessner C (1999) Cell type specific upregulation of vascular endothelial growth factor in an MCA-occlusion model of cerebral infarct. *J Neuropathol Exp Neurol* 58:654–66

Renic M, Kumar SN, Gebremedhin D, Florence MA, Gerges NZ, Falck JR, Harder DR, Roman RJ (2012) Protective effect of 20-HETE inhibition in a model of oxygen-glucose deprivation in hippocampal slice cultures. *J Physiol Heart Circ Physiol* 302:H1285–93

Roman RJ (2002) P-450 metabolites of arachidonic acid in the control of cardiovascular function. *Physiol Rev* 82:131–85

Sehgal N, Agarwal V, Valli RK, Joshi SD, Antonovic L, Strobel HW, Ravindranath V (2011) Cytochrome P4504f, a potential therapeutic target limiting neuroinflammation. *Biochem Pharmacol* 82:53–64

Snider NT, Nast JA, Tesmer LA, Hollenberg PF (2009) A cytochrome P450-derived epoxygenated metabolite of anandamide is a potent cannabinoid receptor 2-selective agonist. *Mol Pharmacol* 75:965–72

Strömstedt M, Warner M, Gustafsson JA (1994) Cytochrome P450s of the 4A subfamily in the brain. *J Neurochem* 63:671–6

Tanaka Y, Omura T, Fukasawa M, Horiuchi N, Miyata N, Minagawa T, Yoshida S, Nakaike S (2007) Continuous inhibition of 20-HETE synthesis by TS-011 improves neurological and functional outcomes after transient focal cerebral ischemia in rats. *Neurosci Res* 59:475–80

Wang JS, Singh H, Zhang F, Ishizuka T, Deng H, Kemp R, Wolin MS, Hintze TH, Abraham NG, Nasjletti A, Laniado-Schwartzman M (2006) Endothelial dysfunction and hypertension in rats transduced with CYP4A2 adenovirus. *Circ Res* 98:962–9

Yang ZJ, Carter EL, Kibler KK, Kwansa H, Crafa DA, Martin LJ, Roman RJ, Harder DR, Koehler RC (2012) Attenuation of neonatal ischemic brain damage using a 20-HETE synthesis inhibitor. *J Neurochem* 121:168–79

Zhang ZG, Zhang L, Tsang W, Soltanian-Zadeh H, Morris D, Zhang R, Goussev A, Powers C, Yeich T, Chopp M (2002) Correlation of VEGF and angiopoietin expression with disruption of blood-brain barrier and angiogenesis after focal cerebral ischemia. *J Cereb Blood Flow Metab* 22:379–92

Supplementary Information accompanies the paper on the Journal of Cerebral Blood Flow & Metabolism website (http://www.nature.com/jcbfm)